

Probability of afternoon precipitation in eastern United States and Mexico enhanced by high evaporation

Kirsten L. Findell^{1*}, Pierre Gentine^{2†}, Benjamin R. Lintner^{3†} and Christopher Kerr⁴

Moisture and heat fluxes from the land surface to the atmosphere form a critical nexus between surface hydrology and atmospheric processes, particularly those relevant to precipitation. Although current theory suggests that soil moisture generally has a positive impact on subsequent precipitation, individual studies have shown support both for^{1–4} and against^{5–7} this positive feedback. Broad assessment of the coupling between soil moisture and evapotranspiration, and evapotranspiration and precipitation, has been limited by a lack of large-scale observations. Quantification of the influence of evapotranspiration on precipitation remains particularly uncertain. Here, we develop and apply physically based, objective metrics for quantifying the impacts of surface evaporative and sensible heat fluxes on the frequency and intensity of convective rainfall during summer, using North American reanalysis data. We show that high evaporation enhances the probability of afternoon rainfall east of the Mississippi and in Mexico. Indeed, variations in surface fluxes lead to changes in afternoon rainfall probability of between 10 and 25% in these regions. The intensity of rainfall, by contrast, is largely insensitive to surface fluxes. We suggest that local surface fluxes represent an important trigger for convective rainfall in the eastern United States and Mexico during the summer, leading to a positive evaporation–precipitation feedback.

Observational studies of soil moisture–rainfall interactions generally suffer from insufficient data both spatially and temporally, particularly for soil moisture (SM) and surface turbulent fluxes. In models, the strength of the SM–rainfall feedback depends on model parameterizations and grid resolution^{8–10}. The metrics introduced in the present study constitute powerful diagnostic tools for model intercomparison of simulated land–atmosphere coupling, and for validation of fundamental physical processes incorporated in next-generation earth system models.

Previous work¹¹ identified three necessary conditions for an initial SM anomaly to impact summertime precipitation: (1) the initial SM anomaly must be large; (2) evaporation must be strongly sensitive to SM; and (3) precipitation must be strongly sensitive to evaporation. The first element emphasizes areas with large SM variability, whereas the latter elements emphasize the connection between the land surface and the atmospheric boundary layer (ABL), and the connection between the ABL and overlying free troposphere¹¹. This study emphasizes (3): we demonstrate when

and where the North American Regional Reanalysis dataset (NARR; ref. 12) manifests strong precipitation sensitivity to the relative strengths of latent and sensible heat fluxes from the land surface. The link between surface evapotranspiration (ET) and subsequent precipitation is recognized as a critical and highly uncertain step in the SM–precipitation feedback loop¹³.

The NARR dataset comprises dynamically consistent three-hourly gridded fields from 1979 to 2003 at ~30 km grid spacing¹², providing an extensive testbed for probing mechanistic connections between surface fluxes and subsequent precipitation. NARR is derived from a data assimilation system with precipitation and other near-surface observations assimilated hourly, and atmospheric profiles of temperature, winds, and moisture from rawinsondes and dropsondes assimilated every three hours. Studies documenting the strengths and weaknesses of NARR are discussed in the Supplementary Information. These studies demonstrate that NARR is an improvement over earlier, global reanalysis projects and that it can successfully be used in a wide array of hydrometeorological studies.

The strengths of NARR include its assimilation of precipitation observations and its high spatio-temporal resolution. Precipitation assimilation constrains the diurnal cycle of precipitation, which is poorly captured by current convection schemes; moreover, assimilation of near-surface humidity constrains latent and sensible heat flux partitioning¹⁴, which is often poorly captured by land surface models. Whereas data density and to a lesser extent frequency are comparable for the continental United States (CONUS) and Mexico, the quality and quantity of observations for Canada are limited; we limit consideration here to data south of 50° N.

Our analysis uses daily gridpoint values of the following quantities: early morning convective triggering potential (CTP) and low-level humidity deficit (HI_{low}) to assess the large-scale potential for convective development¹⁵; before-noon evaporative fraction ($EF = \lambda E / (H + \lambda E)$, with λE and H denoting latent and sensible heating, respectively) to assess surface turbulent flux partitioning; and rainfall from noon–6 pm. Temporal offsetting of measurements helps to isolate EF forcing of subsequent precipitation. Further data filtering (described below) removes large-scale influences potentially affecting both EF and precipitation.

Not surprisingly, the likelihood of summertime afternoon rainfall is higher in the humid regions of the NARR domain: Mexico and the southeastern United States show the highest afternoon rainfall probabilities (Supplementary Fig. S1). These

¹Geophysical Fluid Dynamics Laboratory, 201 Forrestal Road, Princeton, New Jersey 08540, USA, ²Department of Applied Physics and Applied Mathematics, Columbia University, 203 SW Mudd, 500 120th Street, New York, New York 10027, USA, ³Department of Environmental Sciences, Rutgers, The State University of New Jersey, 14 College Farm Road, New Brunswick, New Jersey 08901, USA, ⁴University Corporation for Atmospheric Research/GFDL, 201 Forrestal Road, Princeton, New Jersey 08540, USA. [†]These authors contributed equally to this work. *e-mail: kirsten.findell@noaa.gov.

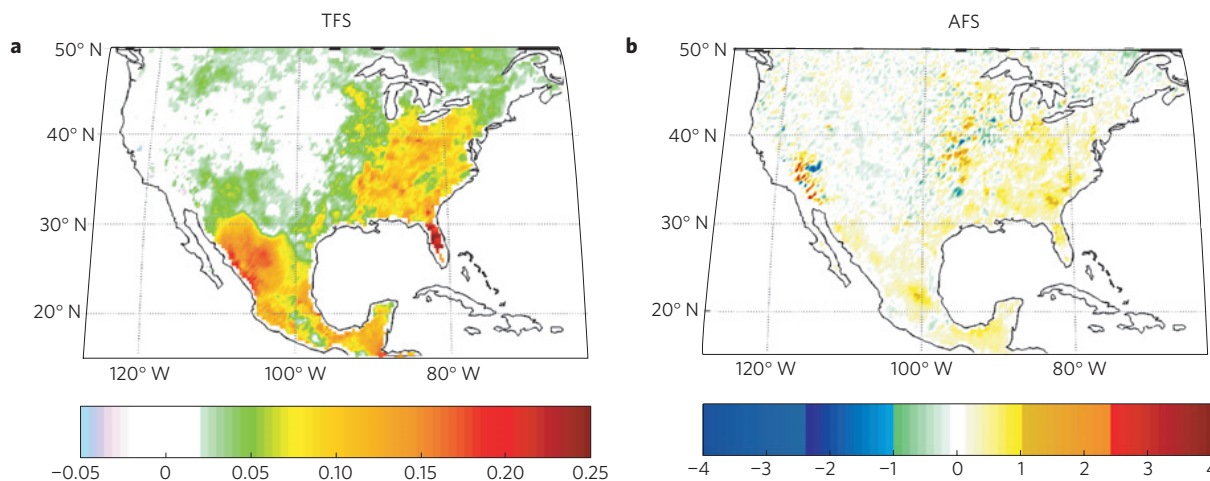


Figure 1 | The sensitivity of convective triggering and rainfall depth to evaporative fraction. a, Triggering feedback strength (TFS; units of probability of afternoon (noon–6 pm) rain) and **b**, amplification feedback strength (AFS; units of millimetres of afternoon rain) during June–July–August (JJA). Mean values from 50 bootstrap samples. Shading indicates the mean of the 50 samples is significantly different from zero according to a two-sided *t*-test at the 95% significance level. This threshold is surpassed by most grid cells because of consistency between the bootstrap samples owing to the large sample size of both the original dataset and each sample member.

regions also show a positive EF–precipitation relationship: higher EF, generally linked to wetter soils and increased vegetation coverage¹⁶, is associated with a higher likelihood of afternoon rainfall (Supplementary Fig. S1).

The EF-dependence of rainfall is assessed through two measures: a triggering feedback strength (TFS), reflecting how afternoon rainfall frequency changes with EF, and an amplification feedback strength (AFS), reflecting how accumulated rainfall varies with EF when afternoon rainfall occurs. TFS is given by

$$\text{TFS} = \sigma_{\text{EF}} \frac{\partial \Gamma(r)}{\partial \text{EF}} \quad (1)$$

where σ_{EF} is the standard deviation of EF. We use Γ to denote event probabilities; $\Gamma(r)$ then denotes the probability of afternoon rain exceeding a 1 mm threshold. AFS is defined analogously, replacing $\Gamma(r)$ with $E[r]$, the expected value of afternoon rainfall amount. (Details are provided in equations (2)–(5) of the Methods section.)

To mitigate the impact of large-scale synoptic systems and constrain the analysis to days when local surface turbulent fluxes are most conducive to subsequent convective development, two restrictions are applied to the data included in TFS. First, only days without rainfall between 6 am and noon are retained, limiting the influence from long-duration stratiform rainfall events¹⁷. Second, days with negative CTP are excluded as early morning CTP < 0 conditions have been shown to be typically too stable to support convection¹⁵; afternoon rainfall occurring on such days is assumed to arise from synoptic-scale systems. These restrictions remove 10–30% of days in the eastern United States and 5–10% in the western United States and northern Mexico (Supplementary Fig. S2). Although these restrictions do not guarantee removal of all synoptically driven days, they diminish the influence of synoptic systems. The AFS calculation is further restricted to days with afternoon rain (Supplementary Fig. S2), because TFS already accounts for rain-free afternoons. Finally, 50 bootstrap samples (with replacement)¹⁸ are created from the available 2,300 days to assess statistical significance.

The TFS map (Fig. 1a) shows that over the eastern United States and Mexico, higher EF leads to increased afternoon rainfall probabilities. This map is largely consistent with Findell and Eltahir¹⁹. Although the earlier study was limited in scope, using station radiosondes in a 1D boundary layer model, simulations

were performed with very dry or wet soils to isolate land surface forcing. Consistency with Findell and Eltahir, in the area they deemed a positive feedback region, supports our finding that surface flux partitioning plays an integral role in afternoon convective triggering in the eastern United States. Independent results from the Atmospheric Radiation Measurement Climate Research Facility Southern Great Plains site (97.5° W, 36.5° N; ref. 20) also show consistency with our near-zero TFS signal at this location.

Figure 1a indicates that EF variability explains 10–20% of the observed variability in afternoon convection probability over most of the eastern United States and Mexico, with peaks over 25% in Florida. This positive land–atmosphere feedback can perpetuate wet or dry extremes by modulating the frequency of afternoon convection. Higher EF, generally associated with higher SM, enhances the probability of daily afternoon rainfall triggering by up to 25%.

In contrast to TFS, the AFS map (Fig. 1b) indicates that, once triggered, the afternoon rainfall intensity is rather insensitive to EF. Where TFS is highest, higher EF may lead to depth increases of < 1 mm (typically < 10% of mean afternoon rainfall, Supplementary Fig. S2). Figure 1 underscores the importance of land surface and ABL processes for convective triggering in some regions while indicating that rainfall amounts are largely independent of local surface moisture conditions in all but the wettest regions.

Thus, in Mexico and the eastern United States, we argue that the positive EF–precipitation feedback occurs primarily through modification of afternoon rainfall frequency. West of the Mississippi, the land surface exerts little control on local afternoon convection. In other words, where surface moisture is not strictly limited, surface turbulent flux partitioning can shift the local atmosphere from non-convecting to convecting, but other controls, for example, free tropospheric moisture content or large-scale moisture convergence, largely determine how much rainfall occurs, consistent with independent studies²¹. The dichotomy between surface controls on convective frequency and intensity constitutes a fundamental advancement in our understanding of land–atmosphere interactions and is consistent with findings from small-scale studies in the US midwest and Europe^{3,17,22}.

To address whether our results reflect external factors that might impact both morning EF and subsequent precipitation we analysed rainfall for the three subsequent six-hourly periods after the noon–6 pm period considered previously. Figure 2

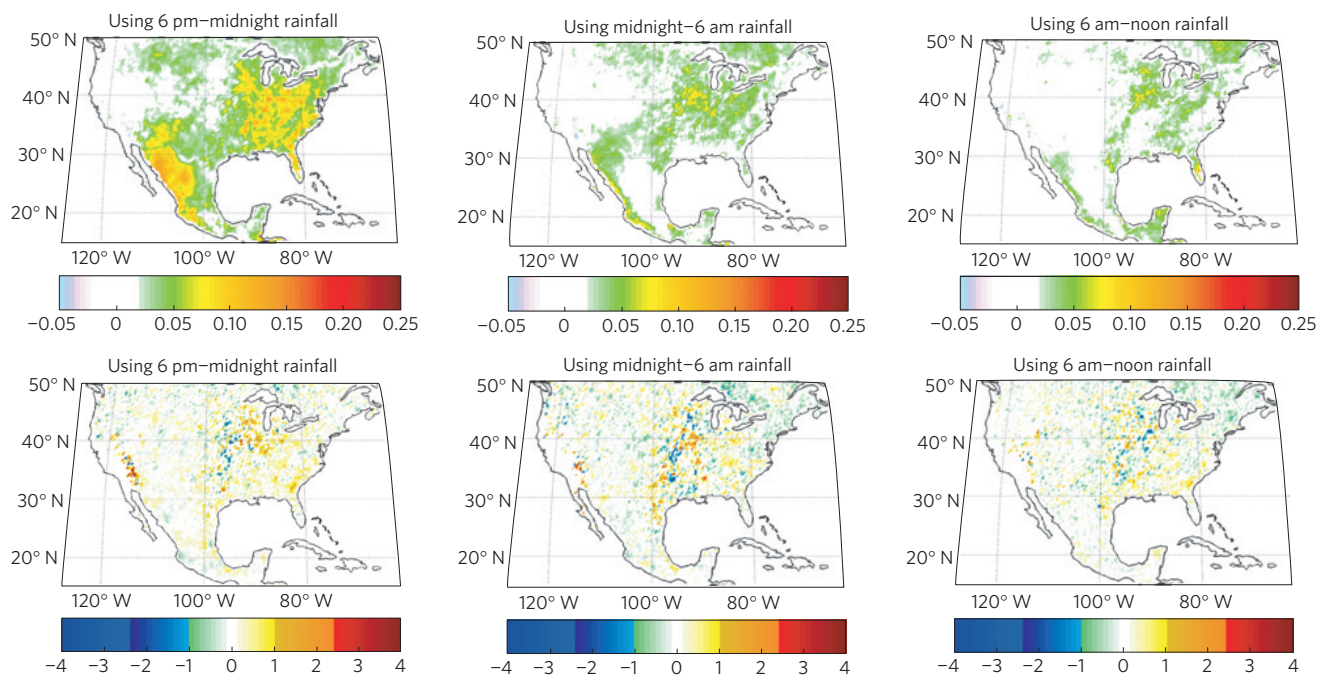


Figure 2 | The sensitivity of TFS and AFS to rainfall time period. TFS (top row) and AFS (bottom row) values calculated using rainfall from subsequent time periods: 6 pm—midnight (left column), midnight—6 am (middle column), and 6 am—noon (right column). The middle and right columns use rainfall from the day following the recorded EF value. Shading details as in Fig. 1.

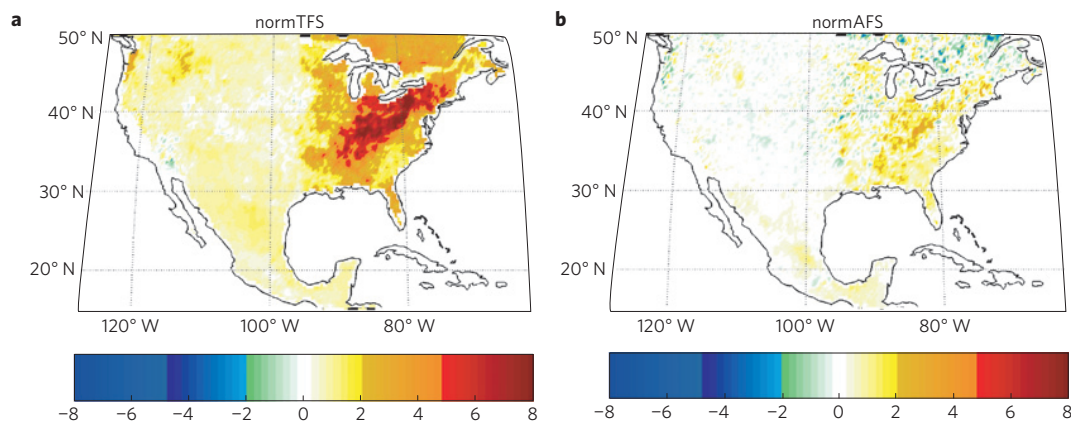


Figure 3 | Normalized, non-dimensional versions of sensitivity maps. **a**, normTFS and **b**, normAFS. Shading details as in Fig. 1.

shows that the TFS signal persists, but is muted from 6 pm to midnight, and drops off rapidly thereafter, with only small areas exceeding 2.5% after 6 am, indicating that persistent large-scale factors do not drive the Fig. 1 results. AFS remains noisy throughout these subsequent intervals, reflecting the difficulty of distinguishing AFS signal from noise. Additionally, we subdivided the dataset into ten El Niño and seven La Niña years (see Supplementary Information). Results with these subsamples show that TFS and AFS are insensitive to tropical SST forcing (Supplementary Fig. S3).

The ground-breaking analysis of Koster *et al.*²³ quantified feedback strength in terms of multi-model mean summertime precipitation variability differences of simulations with and without interactive SM. Their central Great Plains ‘hotspot’ clearly differs from the surface flux triggering hotspot east of the Mississippi evident in our Fig. 1a. The different feedback measures considered (EF versus deep SM) partly explain the different locations, as the Koster *et al.* hotspots include not only the precipitation sensitivity to evapotranspiration considered here, but also evapotranspiration

sensitivity to SM. There were tremendous inter-model differences in the assessment of the SM-precipitation feedback strength in the Koster *et al.* results, tied to model-specific relationships between SM and evapotranspiration⁸ and possibly also the details of convection schemes and cloud-radiative feedbacks²⁴. A related set of experiments with all prognostic land variables (SM and temperature at all levels, canopy interception reservoir content, various snow-related quantities)²⁵ prescribed may be a closer analogue to our work because EF is substantially influenced by surface SM and canopy interception; these experiments manifest a larger signal in the eastern United States, albeit with substantial intermodel differences.

To better understand the relative magnitudes of the triggering and amplification metrics, versions of the TFS and AFS with the central derivatives normalized by the ratio of mean EF (\overline{EF}) to mean rainfall ($\overline{\Gamma(r)}$ or $\overline{E[r]}$) are considered (normTFS and normAFS, see equations (6) and (7) in Methods). Differences between TFS, with derivatives scaled by σ_{EF} , (Fig. 1a) and normTFS (Fig. 3a) are largest in Mexico, where $\overline{\Gamma(r)}$ is highest. The functional

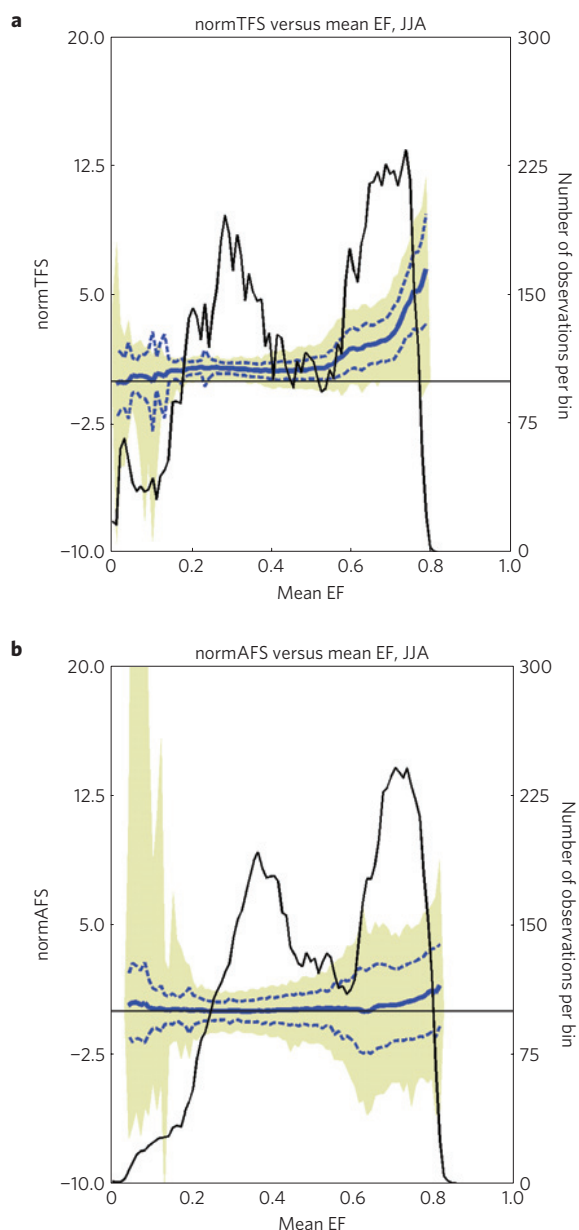


Figure 4 | Functional relationships between normalized metrics and mean evaporative fraction. **a**, normTFS and **b**, normAFS as a function of \overline{EF} (solid blue line) determined from all grid points south of 50° N in each of 50 bootstrap samples. Shaded areas indicate minimum and maximum values of the fifth and ninety-fifth percentile curves from these bootstrap samples; dashed blue lines are the mean $\pm 1\sigma$. The black line indicates the mean number of observations per bin (100 bins with $\Delta EF = 0.01$) over the bootstrap samples. Shading is halted where the mean number of observations/bin < 5 . The pdf of mean number of observations/bin differs in the two plots because only days with afternoon rainfall are included in the AFS calculation.

relationship of normTFS to \overline{EF} is nonlinear but relatively smooth (Fig. 4a). Four regimes are evident: for $\overline{EF} < 0.2$, normTFS is highly variable with a near-zero mean; for $0.2 < \overline{EF} < 0.5$, normTFS shows little change with \overline{EF} ; for $0.5 < \overline{EF} < 0.7$, normTFS shows a slight positive slope with respect to \overline{EF} ; and for $\overline{EF} > 0.7$, normTFS increases dramatically with \overline{EF} . The only instances of negative TFS values are localized to the area north of the Gulf of California (Fig. 3a), reminiscent of a similarly located negative feedback region seen in earlier work¹⁹. For \overline{EF} in the range of

0.2–0.8, almost the entire envelope of normTFS values in 50 bootstrap samples is positive, suggesting that all but the driest regions consistently exhibit a slight positive triggering feedback between daytime \overline{EF} and subsequent convective rainfall. The \overline{EF} -dependence is qualitatively consistent with studies based on idealized coupled boundary layer-free troposphere convecting column models²⁶. These results further indicate that in high- \overline{EF} regimes, typically areas with more dense vegetation and wetter soils, the land surface and atmosphere are tightly coupled. Consequently, wet initial surface conditions are more likely to persist by engendering a greater likelihood of afternoon convection. The results for normAFS demonstrate that the triggering effect is far stronger than the amplification effect at all locations (Figs 3b and Fig. 4b). The functional relationships depicted in Fig. 4 represent powerful diagnostics for model assessment and process-based understanding of surface energy flux partitioning controls on precipitation.

The TFS and AFS metrics estimated from the NARR dataset lead to two important conclusions; TFS indicates substantial local turbulent surface flux partitioning control on the frequency of afternoon convection in areas not strictly limited by surface moisture, whereas AFS indicates a small (< 1 mm-scale) impact on convective rainfall amounts. The distinction between surface flux impacts on rainfall frequency and intensity is relevant to model development. Models often simulate reasonable rainfall climatologies despite incorrect frequency and intensity statistics: many exhibit persistent low-intensity events rather than more intermittent, higher intensity ones²⁷. Improper model representation of land–atmosphere coupling may account for some of these deficiencies over land; the metrics introduced here provide a tool for validating modelled land–atmosphere coupling. This is particularly valuable for improving forecasts of hydroclimatic extremes, comparing land–atmosphere interactions across models, and refining model representations of coupled land–atmosphere processes. Such process-based knowledge is critical for improving future climate prediction capability, for which stationary statistical assumptions based on past or current climate are questionable²⁸ and areas of strong land–atmosphere coupling are likely to change²⁹.

Methods

For each grid point, 2,300 summertime days are available for analysis (25 years, 92 days in June–July–August, JJA). For each day, the three-hourly data are locally positioned to determine the data points closest to local 3 am, 6 am, ... 9 pm, and midnight. Each data point contains accumulated rainfall depths over the 3-h period, or average values over the 3-h period for other variables. Early morning atmospheric conditions are assessed through two quantities used in previous work¹⁵: the convective triggering potential (CTP) and the low-level humidity deficit (HI_{low}). The CTP is a measure of the energy available for convection in the area of the atmosphere 100–300 hPa above the land surface, which is the pressure interval likely to be critical to the development of the daytime boundary layer. HI_{low} is defined as the sum of the dew-point depressions 50 and 150 hPa above the land surface. CTP and HI_{low} are determined from the 6 am observation, capturing the state of the low-level atmosphere before sunrise (from 3 to 6 am).

The energy partitioning at the land surface is assessed through the use of the evaporative fraction (EF), defined as the ratio of latent heat flux (evapotranspiration), λE , to sensible (H) and latent heat fluxes at the surface: $EF = \lambda E / (H + \lambda E)$. We use EF because it has been shown to be relatively constant during daytime hours, and is little affected by turbulence variability³⁰. EF values are calculated for the noontime observation (9 am–noon). Afternoon rainfall is defined over the 6-h period following the noontime EF observation.

The triggering feedback strength (TFS) is a measure of how the probability of afternoon rainfall, $\Gamma(r)$, where r is afternoon rain, changes with EF. Rainfall is ‘triggered’ when afternoon rainfall exceeds a small threshold value, currently set to 1 mm. The results show little qualitative sensitivity to a doubling or halving of this threshold: the location and the relative strength of the high TFS signal does not change, although the quantitative strength of the TFS is slightly impacted by these variations. The amplification feedback strength (AFS) seems to be noisier at lower threshold values.

We treat EF, HI_{low} and CTP as discrete random variables, with the parameter space of these variables divided into discrete bins. The CTP and HI_{low} thresholds

for these bins are pre-defined so that results can be interpreted in the context of the CTP- HI_{low} framework. The EF bins, however, are specific to each grid point: they are determined by splitting the observed range of EF data into 10 bins with an equal number of data points in each bin. For each CTP- HI_{low} pair, the probability of afternoon rainfall for each EF bin is expressed as:

$$\Gamma(r|x, y, \zeta) \triangleq \Gamma(r|x \leq CTP < x + \Delta x, y \leq HI < y + \Delta y, \zeta \leq EF < \zeta + \Delta \zeta) \quad (2)$$

We use the more concise notation format on the left of the above equation in subsequent equations. We take advantage of properties of conditional probabilities to calculate the dependence of afternoon rainfall on EF, considering all CTP- HI_{low} pairs within each EF bin:

$$\begin{aligned} & \frac{\partial \Gamma(r)}{\partial EF} \\ &= \frac{\partial}{\partial EF} \sum_{\zeta=1}^{\zeta_{max}} \Gamma(r, \zeta) \\ &= \frac{\partial}{\partial EF} \sum_{\zeta=1}^{\zeta_{max}} \Gamma(r|\zeta) \Gamma(\zeta) \\ &= \frac{\partial}{\partial EF} \sum_{x=1}^{x_{max}} \sum_{y=1}^{y_{max}} \sum_{\zeta=1}^{\zeta_{max}} \Gamma(r, x, y|\zeta) \Gamma(\zeta) \\ &= \sum_{x=1}^{x_{max}} \sum_{y=1}^{y_{max}} \sum_{\zeta=1}^{\zeta_{max}} \frac{\partial}{\partial EF} [\Gamma(r|x, y, \zeta) \Gamma(x, y|\zeta) \Gamma(\zeta)] \\ &= \sum_{x=1}^{x_{max}} \sum_{y=1}^{y_{max}} \sum_{\zeta=1}^{\zeta_{max}} \left[\Gamma(x, y|\zeta) \Gamma(\zeta) \frac{\partial}{\partial EF} \Gamma(r|x, y, \zeta) + \Gamma(r|x, y, \zeta) \right. \\ & \quad \left. \times \left[\Gamma(x, y|\zeta) \frac{\partial}{\partial EF} \Gamma(\zeta) + \Gamma(\zeta) \frac{\partial}{\partial EF} \Gamma(x, y|\zeta) \right] \right] \end{aligned} \quad (3)$$

To obtain TFS, this derivative is multiplied by σ_{EF} , where σ_{EF} is the standard deviation of EF (see equation (1)). The TFS calculation includes only those days with no rainfall between 6 am and noon and with positive CTP values.

Furthermore, we wish to consider how the expected value of rainfall changes with EF, considering all CTP- HI_{low} pairs. Using a property of the expected value of a positive function, we can represent the expected value in terms of probabilities:

$$\begin{aligned} & \frac{\partial E[R]}{\partial EF} \\ &= \frac{\partial}{\partial EF} \left(\int_{r \geq 0}^{\infty} \Gamma(R \geq r) dr \right) \\ &= \frac{\partial}{\partial EF} \left(\sum_{\zeta=1}^{\zeta_{max}} \int_{r \geq 0}^{\infty} \Gamma(R \geq r|\zeta) \Gamma(\zeta) dr \right) \\ &= \frac{\partial}{\partial EF} \left(\int_{r \geq 0}^{\infty} \sum_{x=1}^{x_{max}} \sum_{y=1}^{y_{max}} \sum_{\zeta=1}^{\zeta_{max}} \Gamma(R \geq r, x, y|\zeta) \Gamma(\zeta) dr \right) \\ &= \sum_{x=1}^{x_{max}} \sum_{y=1}^{y_{max}} \sum_{\zeta=1}^{\zeta_{max}} \frac{\partial}{\partial EF} \left(\int_{r \geq 0}^{\infty} \Gamma(R \geq r|x, y, \zeta) \Gamma(x, y|\zeta) \Gamma(\zeta) dr \right) \\ &= \sum_{x=1}^{x_{max}} \sum_{y=1}^{y_{max}} \sum_{\zeta=1}^{\zeta_{max}} \frac{\partial}{\partial EF} \left(\Gamma(x, y|\zeta) \Gamma(\zeta) \int_{r \geq 0}^{\infty} \Gamma(R \geq r|x, y, \zeta) dr \right) \\ &= \sum_{x=1}^{x_{max}} \sum_{y=1}^{y_{max}} \sum_{\zeta=1}^{\zeta_{max}} \left[\Gamma(x, y|\zeta) \Gamma(\zeta) \frac{\partial}{\partial EF} \int_{r \geq 0}^{\infty} \Gamma(R \geq r|x, y, \zeta) dr \right. \\ & \quad \left. + \int_{r \geq 0}^{\infty} \Gamma(R \geq r|x, y, \zeta) dr \right. \\ & \quad \left. \times \left[\Gamma(x, y|\zeta) \frac{\partial}{\partial EF} \Gamma(\zeta) + \Gamma(\zeta) \frac{\partial}{\partial EF} \Gamma(x, y|\zeta) \right] \right] \\ &= \sum_{x=1}^{x_{max}} \sum_{y=1}^{y_{max}} \sum_{\zeta=1}^{\zeta_{max}} \left[\Gamma(x, y|\zeta) \Gamma(\zeta) \frac{\partial}{\partial EF} E[R|x, y, \zeta] + E[R|x, y, \zeta] \right. \\ & \quad \left. \times \left[\Gamma(x, y|\zeta) \frac{\partial}{\partial EF} \Gamma(\zeta) + \Gamma(\zeta) \frac{\partial}{\partial EF} \Gamma(x, y|\zeta) \right] \right] \end{aligned} \quad (4)$$

This allows us to define the amplification feedback strength (AFS) in an analogous manner to the TFS:

$$AFS = \sigma_{EF} \frac{\partial E[r]}{\partial EF} \quad (5)$$

where $E[r]$ is the expected value of afternoon rainfall amount. The data used in the AFS calculation are further limited to include only days when afternoon rainfall does occur.

Normalized versions of the TFS and AFS are given by scaling the computed derivatives by the ratio of the relevant mean values:

$$\text{normTFS} = \frac{\overline{EF}}{\overline{\Gamma(r)}} \frac{\partial \Gamma(r)}{\partial EF} = \frac{\overline{EF}/\overline{\Gamma(r)}}{\sigma_{EF}} \text{TFS} \quad (6)$$

Similarly,

$$\text{normAFS} = \frac{\overline{EF}}{E[r]} \frac{\partial E[r]}{\partial EF} = \frac{\overline{EF}/E[r]}{\sigma_{EF}} \text{AFS} \quad (7)$$

Received 8 October 2010; accepted 5 May 2011; published online 5 June 2011

References

- Koster, R. D., Suarez, M. J., Higgins, R. W. & Van den Dool, H. M. Observational evidence that soil moisture variations affect precipitation. *Geophys. Res. Lett.* **30**, 1241 (2003).
- Findell, K. L. & Eltahir, E. A. B. An analysis of the soil moisture-rainfall feedback, based on direct observations from Illinois. *Water Resour. Res.* **33**, 725–735 (1997).
- D’Odorico, P. & Porporato, A. Preferential states in soil moisture and climate dynamics. *Proc. Natl Acad. Sci. USA* **101**, 8848–8851 (2004).
- Clark, D. B., Taylor, C. M. & Thorpe, A. J. Feedback between the land surface and rainfall at convective length scales. *J. Hydrometeorol.* **5**, 625–639 (2004).
- Georgakakos, K. P., Bae, D.-H. & Cayan, D. R. Hydroclimatology of continental watersheds, 1. Temporal analysis. *Water Resour. Res.* **31**, 655–675 (1995).
- Cook, B. I., Bonan, G. B. & Levis, S. Soil moisture feedbacks to precipitation in southern Africa. *J. Clim.* **19**, 4198–4206 (2006).
- Giorgi, F., Mearns, L. O., Shields, C. & Mayer, L. A regional model study of the importance of local versus remote controls of the 1988 drought and the 1993 flood over the central United States. *J. Clim.* **9**, 1150–1162 (1996).
- Guo, Z. *et al.* GLACE: The global land-atmosphere coupling experiment. Part II: Analysis. *J. Hydrometeorol.* **7**, 611–625 (2006).
- Mahanama, S. P. P. & Koster, R. D. AGCM biases in evaporation regime: Impacts on soil moisture memory and land-atmosphere feedback. *J. Hydrometeorol.* **6**, 656–669 (2005).
- Hohenegger, C., Brockhaus, P., Bretherton, C. S. & Schär, C. The soil moisture-precipitation feedback in simulations with explicit and parameterized convection. *J. Clim.* **22**, 5003–5020 (2009).
- Koster, R. D. & Suarez, M. J. Impact of land surface initialization on seasonal precipitation and temperature prediction. *J. Hydrometeorol.* **4**, 408–423 (2003).
- Mesinger, F. *et al.* North American regional reanalysis. *Bull. Am. Meteorol. Soc.* **87**, 343–360 (2006).
- Seneviratne, S. I. *et al.* Investigating soil moisture-climate interactions in a changing climate: A review. *Earth Sci. Rev.* **99**, 125–161 (2010).
- Mahfouf, J.-F. Analysis of soil moisture from near-surface parameters—a feasibility study. *J. Appl. Meteorol.* **30**, 1534–1547 (1991).
- Findell, K. L. & Eltahir, E. A. B. Atmospheric controls on soil moisture-boundary layer interactions: Part I: Framework development. *J. Hydrometeorol.* **4**, 552–569 (2003).
- Betts, A. K. Land-surface-atmosphere coupling in observations and models. *J. Adv. Model. Earth Syst.* **1**, 4 (2009).
- Alfieri, L., Claps, P., D’Odorico, P., Laio, F. & Over, T. M. An analysis of the soil moisture feedback on convective and stratiform precipitation. *J. Hydrometeorol.* **9**, 280–291 (2008).
- Von Storch, H. & Zwiers, F. W. *Statistical Analysis in Climate Research* (Cambridge Univ. Press, 1999).
- Findell, K. L. & Eltahir, E. A. B. Atmospheric controls on soil moisture-boundary layer interactions: Part II: Feedbacks within the continental United States. *J. Hydrometeorol.* **4**, 570–583 (2003).
- Zhang, Y. & Klein, S. A. Mechanisms affecting the transition from shallow to deep convection over land: Inferences from observations of the diurnal cycle collected at the ARM Southern Great Plains site. *J. Atmos. Sci.* **67**, 2943–2959 (2010).

21. Romps, D. M. & Kuang, Z. Nature versus Nurture in Shallow Convection. *J. Atmos. Sci.* **67**, 1655–1666 (2010).
22. Schär, C., Lüthi, D., Beyerle, U. & Heise, E. The soil-precipitation feedback: A process study with a regional climate model. *J. Clim.* **12**, 722–741 (1999).
23. Koster, R. *et al.* Regions of strong coupling between soil moisture and precipitation. *Science* **305**, 1138–1140 (2004).
24. Lintner, B. R. & Neelin, J. D. Soil moisture impacts on convective margins. *J. Hydrometeorol.* **10**, 1026–1039 (2009).
25. R, Koster *et al.* GLACE: The global land–atmosphere coupling experiment. Part I: Overview. *J. Hydrometeorol.* **7**, 590–610 (2006).
26. De Ridder, K. Land surface processes and the potential for convective precipitation. *J. Geophys. Res.* **102**, 30085–30090 (1997).
27. Lin, J. W. B. & Neelin, J. D. Toward stochastic deep convective parameterization in general circulation models. *Geophys. Res. Lett.* **30**, 1162 (2003).
28. Milly, P. C. D. *et al.* Stationarity is dead: Whither water management? *Science* **319**, 573–574 (2007).
29. Seneviratne, S. I., Lüthi, D., Litschi, M. & Schär, C. Land–atmosphere coupling and climate change in Europe. *Nature* **443**, 205–209 (2006).
30. Crago, R. & Brutsaert, W. Daytime evaporation and the self-preservation of the evaporative fraction and the Bowen ratio. *J. Hydrolol.* **178**, 241–255 (1996).

Acknowledgements

We thank R. Stouffer, S. Malyshev, F. D’Andrea, S. Seneviratne and A. Berg for providing comments on the manuscript. We thank A. Wittenberg for help with the determination of ENSO years. P.G. and B.R.L. are supported by an NSF grant and B.R.L. is also supported by a NOAA grant and an NJAES Hatch grant. National Centers for Environmental Prediction (NCEP) North American Regional Reanalysis (NARR) data provided by the National Climatic Data Center from their website: <http://nomads.ncdc.noaa.gov/data.php>.

Author contributions

K.L.F. performed the analysis of the data and wrote the paper. K.L.F., P.G. and B.R.L. jointly designed and refined the study. P.G. and B.R.L. contributed equally to the work. C.K. converted the original data to netCDF format. All authors discussed the results and commented on the manuscript.

Additional information

The authors declare no competing financial interests. Supplementary information accompanies this paper on www.nature.com/naturegeoscience. Reprints and permissions information is available online at <http://www.nature.com/reprints>. Correspondence and requests for materials should be addressed to K.L.F.